HHS Public Access

Author manuscript

Nat Chem Biol. Author manuscript; available in PMC 2017 January 04.

Published in final edited form as:

Nat Chem Biol. 2016 September ; 12(9): 672–679. doi:10.1038/nchembio.2115.

Sensitivity and engineered resistance of myeloid leukemia cells to BRD9 inhibition

Anja F. Hohmann[1,2], **Laetitia J. Martin**[3], **Jessica Minder**[1], **Jae-Seok Roe**[1], **Junwei Shi**[1,4], **Steffen Steurer**[3], **Gerd Bader**[3], **Darryl McConnell**[3], **Mark Pearson**[3], **Thomas Gerstberger**[3], **Teresa Gottschamel**[3], **Diane Thompson**[3], **Yutaka Suzuki**[5], **Manfred Koegl**[3], and **Christopher R. Vakoc**[1,2]

[1]Cold Spring Harbor Laboratory, Cold Spring Harbor, New York, U.S.A

[2]Watson School of Biological Sciences, Cold Spring Harbor Laboratory, Cold Spring Harbor, New York, U.S.A

[3]Boehringer Ingelheim Regional Center Vienna GmbH and Company KG, Vienna, Austria

[4]Molecular and Cellular Biology Program, Stony Brook University, Stony Brook, New York, U.S.A

[5]Department of Medical Genome Sciences, University of Tokyo, Kashiwa, Chiba 277-8562, Japan

Abstract

Here we show that acute myeloid leukemia (AML) cells require the BRD9 subunit of the SWI/SNF chromatin remodeling complex to sustain *MYC* transcription, rapid cell proliferation, and a block in differentiation. Based on these observations, we derived small-molecule inhibitors of the BRD9 bromodomain, which selectively suppressed the proliferation of mouse and human AML cell lines. To establish these effects as on-target, we engineered a bromodomain-swap allele of *BRD9*, which retains functionality despite a radically altered bromodomain pocket. Expression of this allele in AML cells conferred resistance to the anti-proliferative effects of our compound series, thus establishing BRD9 as the relevant cellular target. Furthermore, we used an analogous domain-swap strategy to generate an inhibitor-resistant allele of *EZH2*. Our study provides the first evidence for a role of BRD9 in cancer and reveals a simple genetic strategy for constructing resistance alleles to demonstrate on-target activity of chemical probes in cells.

Correspondence to: Christopher R. Vakoc.

Accession codes

All RNA-seq and ChIP-seq datasets will be available at GEO accession XXXXX.

Author Contributions

A.F.H., L.J.M., M.K., C.R.V. designed experiments and analyzed results; A.F.H. and J.M. performed genetic characterization of BRD9, cellular evaluation of BRD9 inhibitors and domain-swap studies; J-S.R. performed ChIP-Seq; J.S. performed IP-MS; L.J.M., S.S., G.B., T. Ge., T. Go., D.T., M.K. derived BRD9 inhibitors, carried out *in vitro* characterization and human cell line sensitivity profiling; Y.S. prepared and sequenced shRen and shBrd9 RNA-Seq libraries; L.J.M., D.M., M.P., M.K., C.R.V. supervised the research; A.F.H., L.J.M., C.R.V. wrote the manuscript.

Competing financial interests

This study was funded in part via a sponsored research agreement with Boerhinger Ingelheim.

Introduction

Chemical probes have proven to be powerful complements to genetic approaches in revealing basic protein function and therapeutic opportunities[1–3]. A particular challenge in developing tool compounds lies in achieving selectivity, both within a family of conserved protein domains and across the diverse proteome of the cell[3]. As a consequence, chemical compounds frequently bind more than a single protein. While biochemical methods exist to identify the binding partners of a small-molecule, such approaches offer little insight into the physiological relevance of the identified interactions[4]. Strong support for a physiologically important drug-target interaction is lent by naturally arising or engineered mutations in a target protein that confer resistance to a compound of interest[3]. While such mutants have been successfully used in the study of kinase inhibitors (e.g. gatekeeper mutations), a genetic strategy has yet to be devised to establish the relevant targets of the expanding class of chromatin-modulating small molecules[5].

Prominent among chromatin regulator drug targets are bromodomain-containing proteins[6]. Bromodomains are chromatin reader modules that engage in acetyl-lysine recognition and are found in a diverse array of transcriptional coactivators and chromatin regulators[7]. The human bromodomain family encompasses 61 domains, found on 46 proteins. Large-scale biochemical assays have revealed that individual bromodomains have distinct binding preferences for acetyl-lysine containing peptides, which implies functional specialization among these proteins in the cell[8].

The deep bromodomain pocket can be targeted with small-molecules[7,9]. Inhibitors of BET (bromodomain and extra-terminal domain) proteins, such as JQ1 and I-BET, bind their target bromodomains in an acetyl-lysine competitive manner, leading to the displacement of BET proteins from chromatin[10,11]. These inhibitors are promising antitumor agents for a variety of cancers, in particular hematopoietic malignancies[12]. The pharmacological tractability of BET bromodomains has prompted efforts to develop compounds targeting other bromodomain-containing proteins to explore biological activities and therapeutic potential. As a result, bromodomains outside of the BET family, such as those of CBP, BAZ2B, and TRIM24 have now also been successfully targeted[13–15]. Due to the structural similarities of bromodomains and the conservation of acetyl-lysine binding residues, however, generating inhibitors that selectively interfere with a single bromodomain has proven to be challenging, which complicates the assignment of phenotypic effects to a specific bromodomain target[10,11]. Genetic approaches to pinpoint the key target(s) of a bromodomain inhibitor in the cell are currently lacking. Analogous to kinase gatekeeper mutations, bromodomain alleles that retain functionality while disrupting small-molecule inhibition would prove immensely useful in discriminating on-target from off-target effects in cells.

Recent studies have implicated the multi-subunit SWI/SNF chromatin remodeling complex as a therapeutic target in various malignancies, including acute myeloid leukemia (AML)[16–20]. In certain AML contexts, it has been shown that the SWI/SNF ATPase subunit BRG1 performs an essential function by supporting enhancer-mediated *Myc* expression[16]. However, strategies to inhibit this function pharmacologically have yet to be achieved. An alternative approach to exploit the SWI/SNF-dependence of AML cells would be to target

other subunits within the complex. While SWI/SNF composition varies depending on tissue and cell type[21], numerous subunits with potentially targetable chromatin reader domains have been described, including five bromodomain-containing subunits (BRG1, BRM, PBRM1, BRD7, and BRD9). The bromodomain of BRG1 has been shown to be dispensable for its leukemia maintenance function[16,22], however the role of the other bromodomain proteins remains to be investigated in this disease context.

Here we show that BRD9 is a subunit of SWI/SNF complexes in AML cells and that it uses a bromodomain pocket to promote *MYC* expression and cell proliferation in this context. Based on these findings we derived novel small-molecule bromodomain inhibitors that target BRD9 and these compounds are shown to selectively limit the proliferation rate of AML cell lines. Remarkably, we discovered that the bromodomain of BRD9 can be replaced with other bromodomains without compromising its essential function in leukemia cells. This observation allowed us to derive a *BRD9* bromodomain-swap allele, which we use to pinpoint BRD9 as the relevant target underlying the anti-leukemia effects of our small-molecule series. Our findings implicate BRD9 as a key constituent of SWI/SNF complexes in AML and reveal domain-replacement as a general strategy for defining the relevant cellular target of chemical probes.

Results

BRD9 is a SWI/SNF subunit that supports AML cell growth

Direct chemical inhibition of BRG1 in cancer cells has yet to be achieved. Therefore, we pursued a strategy of indirect BRG1 modulation by targeting subunits of its associated SWI/SNF complex. As SWI/SNF composition is known to vary depending on cell type, we sought to define BRG1-associated SWI/SNF subunits in AML cells[21]. Immunoprecipitation of endogenous BRG1 from human AML cell line nuclear lysates followed by iTRAQ mass spectrometry recovered BRD9, which is a largely unstudied bromodomain-containing protein recently identified as a SWI/SNF subunit (Fig. 1a)[23,24]. This result was unexpected, since a prior report found that Brd9 was absent from SWI/SNF complexes isolated from murine leukemia cells, which instead contained the Brd9 homolog, Brd7[17]. However, our ChIP-seq analysis of Brg1 and Brd9 chromatin occupancy in murine MLL-AF9/Nras^{G12D} AML cells (RN2 cell line)[25] revealed a striking similarity across the genome at acetylated promoters and enhancers, consistent with both proteins existing in one complex (Fig. 1b, 1c). In addition, Brd9 was significantly enriched at a distal cluster of enhancers (or super-enhancer) located 1.7 Mb downstream of the *Myc* promoter, which are elements through which Brg1 regulates *Myc* expression in this cell type (Fig. 1c and Supplementary Results, Supplementary Fig. 1)[16]. Collectively, these findings suggest that Brd9 is a SWI/SNF subunit in AML.

We next performed functional experiments to evaluate whether Brd9 acts in a similar manner to Brg1 in supporting leukemia maintenance. Using a competition-based proliferation assay, we evaluated the effect of Brd9 knockdown on AML cell growth. RN2 cells transduced with Brd9 shRNAs were rapidly outcompeted by non-transduced cells during culturing (Fig. 2a). In support of these effects occurring as a consequence of Brd9 knockdown, expression of a human *BRD9* cDNA not recognized by the shRNAs targeting murine *Brd9* rescued this

growth-arrest phenotype (Fig. 2b and Supplementary Fig. 2a). In contrast to the effects observed in AML cells, Brd9 knockdown did not influence the growth of immortalized mouse embryonic fibroblasts (iMEFs), which is a similar context-dependence observed previously with Brg1 knockdown (Supplementary Fig. 2b, c)[16]. Knockdown of the Brd9 homolog, Brd7, did not impair RN2 cell expansion (Supplementary Fig. 2d, e). To extend these findings to human cells, we validated shRNAs that decrease human BRD9 expression and assessed their effect on the growth of a panel of 15 human cancer cell lines (Fig. 2c and Supplementary Fig. 2f–h). This analysis revealed that the majority of myeloid leukemia cell lines spanning diverse genetic backgrounds were dependent on BRD9 for cell expansion (Fig. 2c and Supplementary Fig. 2h). In contrast, the growth of several epithelial cancer lines was insensitive to BRD9 knockdown (Fig. 2c). Collectively, these findings suggest a context-dependent Brd9 requirement for the proliferation of AML cells.

BRD9 sustains *Myc* and prevents differentiation in AML

We next evaluated the transcriptional program maintained by Brd9 in AML cells. For this purpose, we performed a deep sequencing analysis of mRNA abundance (RNA-seq) in RN2 cells following 48 hours of Brd9 knockdown, using three independent Brd9 shRNAs compared to a negative control shRNA targeting *Renilla* luciferase. As expected based on the Brd9 ChIP-seq analysis, *Myc* was among the most down-regulated mRNAs following Brd9 knockdown (Fig. 2d and Supplementary Fig. 3a, b). In addition, we observed altered expression of several genes related to myeloid differentiation (*Mmp9*, *Itgam*, *Mpo*, and *Ccr2*) (Fig. 2d). To systematically characterize Brd9-dependent gene expression in RN2 cells, we applied Gene Set Enrichment Analysis (GSEA) to the RNA-seq dataset[26]. We interrogated 6921 gene signatures: 6917 derived from the Molecular Signatures Database (MSigDB) and 4 from our prior characterization of Brg1-dependent gene expression in RN2 cells (Supplementary Data Set 1)[16]. Among the most enriched gene signatures in this analysis (|Normalized Enrichment Score (NES)| > 2 and FWER p-value = 0) were the downstream target genes of Myc as well as genes upregulated during myeloid differentiation, which were decreased and increased, respectively, upon Brd9 knockdown (Fig. 2e, Supplementary Fig. 3c and Supplementary Tables 1 and 2). In addition, a Brg1-dependent gene signature defined previously in RN2 cells was also suppressed following Brd9 knockdown (NES 2.13, FWER p-value 0.015) (Supplementary Fig. 3c)[16]. These effects were context dependent, since Brd9 knockdown in iMEFs did not influence *Myc* expression or Myc target gene signatures (Supplementary Fig. 3d–g). These findings show that Brd9, like Brg1, is required to maintain a transcriptional program in AML cells that sustains the Myc pathway and blocks myeloid differentiation.

To test whether the observed gene expression changes would manifest as a differentiation phenotype, we used flow cytometry to measure cell surface levels of Kit, which is expressed in undifferentiated hematopoietic cells, and Mac-1 (encoded by *Itgam*), which is upregulated during myeloid maturation. Independent Brd9 shRNAs provoked a decrease in Kit and an increase in Mac-1, which is consistent with the RNA-seq findings (Supplementary Fig. 4a). We also examined May-Grünwald/Giemsa-stained RN2 cells by light microscopy to assess for morphological signs of differentiation (Fig. 2f). Control RN2 cells showed large nuclei and a round cell shape characteristic of leukemic blasts. In contrast, Brd9-deficient cells

contained multilobulated nuclei and vacuolar structures, and possessed an irregular cell shape, consistent with myeloid differentiation (Fig. 2f). Brd9 knockdown in RN2 cells also resulted in a G1-arrest without a significant effect on apoptosis (Supplementary Fig. 4b–d). Based on our prior characterization of Brg1-deficient RN2 cells[16], we suspected that *Myc* suppression would be a key contributor to the differentiation phenotype induced upon Brd9 knockdown. In agreement with this hypothesis, expression of a *Myc* cDNA from a retroviral promoter in RN2 cells prevented myeloid differentiation and the proliferation arrest induced by Brd9 knockdown (Fig. 2f, g). The similar phenotypic effects of Brd9 and Brg1 knockdown, in concert with the IP-MS and ChIP-seq evidence presented above, provide strong support for Brd9 maintaining the leukemia cell state via its presence in the SWI/SNF complex.

The BRD9 bromodomain is essential in AML cells

We next evaluated the importance of the BRD9 bromodomain for its essential role in leukemia. To this end, we employed the shRNA/cDNA complemention assay described above and evaluated the functionality of BRD9 mutants that either completely lack the bromodomain (BRD9ΔBD) or carry an asparagine-to-alanine substitution of a conserved residue that was reported to be critical for acetyl-lysine binding in related bromodomains (BRD9N216A) (Fig. 3a)[27]. In this assay, BRD9ΔBD and BRD9N216A proteins were unable to support RN2 cell proliferation, despite being expressed at comparable levels to wild-type BRD9 (Fig. 3b, Supplementary Fig. 5a, e). Furthermore, we noticed that expression of BRD9ΔBD or BRD9N216A alone was sufficient to reduce *Myc* expression and RN2 cell growth, yet expression of these cDNAs did not impair the proliferation of iMEFs (Supplementary Fig. 5b–d). The similarity of these effects to those observed with shRNA-based Brd9 knockdown suggests that bromodomain-mutant alleles of BRD9 exhibit dominant-negative effects on endogenous Brd9. Experiments performed using CRISPR-Cas9-based mutagenesis directed at the Brd9 bromodomain-encoding exons lend further support for the role of this domain in maintaining RN2 proliferation (Supplementary Fig. 6). Taken together, our findings suggest that bromodomain-mediated acetyl-lysine recognition is a critical function of BRD9 in AML.

A chemical series that targets the BRD9 bromodomain

Our genetic evidence provided rationale for the development of small molecules that interfere with the acetyl-lysine recognition function of the BRD9 bromodomain. Two parallel screening approaches led to the identification of BRD9 bromodomain binding compounds (Supplementary Note 1 and Supplementary Table 5). A generic fragment-based library was screened by differential scanning fluorimetry (DSF), surface plasmon resonance (SPR), and microscale thermophoresis resulting in 77 hits. In parallel, a second library was screened virtually and hits were then tested by DSF and SPR leading to 23 additional candidates. Chemical optimization of the identified hits was guided by co-crystal structures, which were used to improve the shape complementarity of the compounds towards the BRD9 bromodomain. Besides potency for BRD9, these efforts focussed on avoiding binding to BRD4 bromodomains, which are known to be highly active in supporting leukemia cell proliferation[28]. Several rounds of optimization resulted in three potent compounds for the bromodomain of BRD9 (BI-7271 (**1**), BI-7273 (**2**), BI-7189 (**3**); IC50 < 50 nM) with >1,000

fold selectivity over the bromodomains of BRD4, as determined using AlphaScreen assays measuring the binding of acetylated histone peptides to recombinant bromodomains in the presence of increasing compound concentrations (Fig. 3c, d and Supplementary Figs. 7a–d). We further employed the bromoMAX and bromoKdELECT assays to evaluate selectivity of the compounds across the bromodomain family. All three compounds were highly selective for the homologous bromodomains of BRD9 and BRD7 and, to a 10-fold lesser extent, CECR2 (Fig. 3e and data not shown). The crystal structure of BI-7273 bound to the BRD9 bromodomain reveals how the carbonyl group of the isoquinolinone ring interacts with asparagine 216 and further forms a π-stacking interaction with tyrosine 222 (Fig. 3f). The isoquinolinone ring also interacts with a conserved water molecule bound by tyrosine 173 (not shown). Additionally, the dimethoxyphenyl linker adopts a conformation that permits T-stacking with phenylalanine 160 (Fig. 3f and Supplementary Table 6). A lack of binding to BRD4 can be explained by a steric clash of the isoquinolinone moiety of the compounds with the BRD4 bromodomain pocket (data not shown). The synthetic route for all three compounds is provided in Supplementary notes 1 and 2. A more detailed description of the derivation of this compound series is described in a separate study[29].

We next evaluated whether BI-7273 can block the bromodomain function of BRD9 in a cellular environment. Using a nanoBRET assay in HEK293T cells, we confirmed a submicromolar activity of BI-7273 in disrupting the BRD9 bromodomain interaction with histone H3 (Supplementary Fig. 7e)[30]. ChIP-qPCR revealed that exposure to BI-7273 led to a partial reduction of FLAG-BRD9 and Brg1 occupancy at the *Myc* enhancer elements in RN2 cells (Supplementary Fig. 8a, b). While this effect was of modest magnitude, a ChIP-seq analysis revealed that the *Myc* enhancers were among the genomic regions exhibiting the greatest FLAG-BRD9 and Brg1 displacement following BI-7273 exposure (Supplementary Fig. 8c, d). These findings indicate that BI-7273 inhibits BRD9 in a cellular context, though it also appears that SWI/SNF complexes are able to associate with chromatin at many genomic regions in a BRD9-independent manner (Supplementary Fig. 8d)

Domain-swap allele confers resistance to BRD9 inhibition

All three compounds exerted dosage-dependent inhibition of RN2 cell proliferation, with EC50 values ranging from 217–1,784 nM correlating with the relative potency of each molecule for BRD9 inhibition in biochemical assays (Fig. 4a and Supplementary Fig. 7d). By evaluating BI-7273 in a panel of 62 human cancer cell lines, we found that sensitivity to this compound was largely confined to hematopoietic cancers, with AML cell lines being the most sensitive overall (Fig. 4b and Supplementary Fig. 9a, b). These findings are largely in agreement with our genetic profiling of BRD9 dependence in human cancer cell lines (Fig. 2c).

One issue that arises when evaluating the aforementioned compounds lies in determining whether Brd9 is the relevant cellular target that underlies the observed anti-proliferative effects. While our compounds are capable of targeting BRD9, BRD7, and CECR2, our CRISPR-Cas9 and RNAi experiments indicate that only the bromodomain of Brd9 is essential in leukemia cells (Supplementary Fig. 2d, e and Supplementary Fig. 6). However,

RN2 cells have been shown to be highly sensitive to Brd4 bromodomain inhibition[28]. Hence, we were concerned that even a slight off-target activity of our compound series against Brd4 could account for the observed anti-leukemia effects. Additionally, we could not exclude a contributory off-target activity outside of the bromodomain protein family. We therefore considered it paramount to derive a *BRD9* allele that would be insensitive to chemical inhibition yet retain functionality, in analogy to kinase gatekeeper mutations. Such an allele would allow us to evaluate the contribution of Brd9 to the growth-arrest phenotypes caused by our compound series.

During our efforts to evaluate the tolerance of BRD9 to amino acid alterations in its bromodomain pocket, we unexpectedly discovered that the bromodomain of BRD9 can be entirely replaced with other bromodomains without comprising its functionality in leukemia cells. The closest bromodomain homologs of BRD9 are BRD7 and BRD1 (Fig. 3e and Supplementary Fig. 10a). BRD9 variants harboring the bromodomain from either BRD7 or BRD1 were expressed and retained full functionality in supporting RN2 proliferation in the shRNA/cDNA rescue assay (Fig. 4c and Supplementary Fig. 10b, c). To our surprise, we also found that the first bromodomain of BRD4 supported full BRD9 activity in this domain-swap assay, despite its limited sequence and structural similarity to the BRD9 bromodomain (Fig. 4c and Supplementary Fig. 10a–c)[8]. In agreement with this finding, ChIP-qPCR analysis revealed that the BRD4 bromodomain allowed localization of the chimeric BRD9 protein (hereafter referred to as BRD9-BET) to the *Myc* enhancer elements at comparable levels to wild-type BRD9 (Supplementary Fig. 10d). However, other bromodomains (e.g. that of BRG1) failed to support BRD9 function in the domain-swap assay, indicating that only specific bromodomains are interchangeable with that of BRD9 (Supplementary Fig. 10b, c, e). These observations define a domain-swap strategy for producing a functional BRD9 protein possessing a radically altered amino acid composition of its bromodomain module.

The AlphaScreen results showed that our compound series exhibits minimal affinity for BRD4 bromodomains, and therefore should have reduced affinity for BRD9-BET relative to wild type BRD9 (Fig. 3d, e and Supplementary Fig. 7a, b, d). Remarkably, BRD9-BET expression reduced the sensitivity of RN2 cells to all three compounds (Fig. 4d and Supplementary Fig. 10 f, g). In the case of BI-7271 and, to a lesser extent, BI-7189, the rescue effect was partial at higher inhibitor concentrations (Supplementary Fig. 10f, g). In contrast, the BRD9-BET expressing cells were completely resistant to BI-7273 at even the highest concentrations tested (Fig. 4d). These findings establish Brd9 as the sole target underlying the anti-proliferative effects of this molecule in RN2 cells. In addition, use of this allele reveals the superiority of BI-7273 within our chemical series in achieving potent and selective Brd9 inhibition. This assay also allowed us to evaluate the on-target activity of two other recently described BRD9 bromodomain inhibitors, LP99 and I-BRD9[31,32]. Expression of BRD9-BET partially alleviated the growth-arrest caused by I-BRD9, but only minimally influenced the sensitivity of RN2 cells to LP99 (Supplementary Fig. 11), which is in agreement with the relative effect of these compounds on the proliferation of BRD9-dependent versus BRD9-independent cell lines (Supplementary Fig. 9c, d). Taken together, these findings highlight the utility of a bromodomain-swap allele in evaluating on-target effects within a compound series.

Transcriptional effects of chemical BRD9 inhibition

If BI-7273 achieves its primary effect in RN2 cells via Brd9 inhibition, chemical and genetic inhibition of Brd9 should lead to similar transcriptional changes. To evaluate this, we performed RNA-seq analysis following exposure of RN2 cells to 1.25 μM BI-7273 for 24 hours. Notably, among the most altered genes were *Myc*, *Mpo*, *Ccr2*, and *Itgam*, which resembled the gene expression changes observed following Brd9 knockdown (Fig. 5a and Fig. 2d). To further evaluate the similarity of genetic and chemical Brd9 inhibition, we performed GSEA as described above, with the inclusion of two additional gene sets comprising the top 100 up- and down-regulated genes identified in our prior RNA-seq analysis in RN2 cells following Brd9 knockdown (Fig. 2d and Supplementary Data Set 1). Among this large group of genesets, the two Brd9-dependent gene signatures were outliers with regard to the magnitude of perturbation following BI-7273 treatment (Fig. 5b, c). In addition, BI-7273 altered Myc target gene sets and myeloid differentiation signatures similarly to Brd9 knockdown (Fig. 5b, c and Supplementary Fig. 12a). A similar pattern of gene expression changes were also observed when treating RN2 cells with 1 uM I-BRD9, whereas 1 uM LP99 only minimally influenced Brd9-dependent gene expression (Supplementary Fig. 13). These findings are in agreement with results of the bromodomain-swap assay, which revealed on-target effects of I-BRD9 at the 1 uM concentration (Supplementary Fig. 11). Using RNA-seq, we also observed a similar pattern of *MYC* suppression upon treating BRD9-dependent AML cell lines HL-60 and MV4-11 with BI-7273, while no such effect was found in BRD9-independent HeLa and iMEF cells (Fig. 5e–j, Supplementary Fig. 12b–d and Supplementary Fig. 14). In addition, retroviral overexpression of *Myc* reduced the sensitivity of RN2 cells to BI-7273, in accord with *Myc* suppression being a major consequence of both chemical and genetic targeting of Brd9 (Fig. 5d and Fig. 2g). Collectively, these findings indicate that on-target chemical inhibition of Brd9 leads to AML-specific *Myc* suppression and a consequent arrest of rapid cell proliferation.

Domain-swap allele confers resistance to EZH2 inhibition

We next explored whether the domain-swap strategy could be applied to evaluate the on-target effects of other chromatin-modulating chemical probes. Recent studies have characterized small-molecule inhibitors of the EZH1 and EZH2 SET domains, which catalyze histone H3 lysine K27 (H3K27) methylation to repress transcription[33,34]. One such molecule, GSK126, exhibits >150-fold selectivity for EZH2 versus EZH1, despite the 94% identity of the two SET domains (Supplementary Fig. 15a)[35]. Moreover, it has previously been established that MLL-AF9-transformed AML cells are dependent on EZH2, and undergo growth-arrest following exposure to GSK126[36,37]. Based on this, we considered the possibility that expressing a variant of EZH2 harboring the SET domain of EZH1 (hereafter termed $EZH2^{EZH1\text{-}SET}$) in RN2 cells might confer resistance to GSK126. Indeed, while overexpression of wild-type EZH2 minimally influenced the sensitivity of RN2 cells to GSK126, we found that overexpression of $EZH2^{EZH1\text{-}SET}$ rendered the cells resistant to GSK126 at concentrations up to 10 uM (Fig. 6 and Supplementary Fig. 15b). These results confirm the specificity of GSK126 for EZH2 versus EZH1, and establish EZH2 as the single target underlying the effects of this molecule in AML cells. Collectively, the findings in this

study suggest a broader utility for domain-swap alleles in establishing on-target effects of chemical probes.

Discussion

Here we have shown that BRD9 is a unique dependency in hematopoietic cancers, which we have traced to a tissue-specific role for BRD9 in supporting enhancer-mediated *Myc* expression. Our functional experiments suggest that BRD9 is required, at least in part, for tethering SWI/SNF complexes to a subset of cis-regulatory elements in AML cells, however we cannot exclude the possibility that BRD9 performs functions independently of SWI/SNF. Nonetheless, chemical inhibition of BRD9 only results in partial release of SWI/SNF from a subset of *cis* elements, which can be explained by the presence of multiple chromatin binding modules within heterogeneous SWI/SNF complex assemblies in this cell type. Therefore, it is likely that combined targeting of multiple SWI/SNF surfaces will be necessary to achieve complete complex eviction from chromatin. Since chemical modulation of SWI/SNF holds considerable promise as a therapeutic avenue in cancer, future efforts should be directed at defining the full complement of chromatin-binding modules in SWI/SNF, and how such surfaces act in a redundant/compensatory manner with one another. Such an approach may reveal opportunities for combining BRD9 inhibitors with other small-molecules to achieve potent SWI/SNF displacement and consequent therapeutic effects in cancer. An alternative approach might be to target SWI/SNF complexes for proteasome-mediate destruction, which has recently been achieved by conjugating bromodomain inhibitors to E3 ligase targeting ligands[38–40].

The on-target effects of chemical Brd9 inhibition in our study were established by using the BRD9-BET bromodomain-swap allele, which replaces the BRD9 bromodomain with that of the first bromodomain of BRD4. The interchangeability of BRD9 and BRD4 bromodomains in these experiments was unexpected, since these two reader domains exhibit distinct binding preferences for acetylated peptides in biochemical assays and belong to different phylogenetic subfamilies of bromodomain modules[8]. Interestingly however, Brd4, Brd9, and BRD9-BET are each highly enriched at the *Myc* enhancers in AML cells[16]. This leads us to speculate that the distinct ligands of the BRD4 and BRD9 bromodomains in the cell are likely to coexist at the distal *Myc* enhancers in AML cells, which would allow two otherwise divergent reader domain modules to be functionally synonymous.

Our study highlights the use of domain-swap alleles as a chemical-genetic strategy for establishing the relevant protein target underlying the biological effects of a small-molecule. Such a reagent may aid our interpretation of effects of existing chemical probes, particularly those with only partially characterized target selectivity in biochemical assays. In addition, the high attrition rate of drug candidates in clinical development highlights the need for better tools to understand the mechanism of action of chemical inhibitors early during the discovery process[41]. Since minimal biochemical and structural insight into a protein target is required to generate a domain-swap allele, the domain-swap approach can be readily expanded to many targets of small-molecules to aid drug discovery. In this regard, a large-scale effort to define functionally synonymous members within domain families may have potential to greatly expand the chemical-genetic toolkit.

Methods

Immunoprecipitation

To isolate nuclear extracts, NOMO-1 cell pellets were washed in PBS, resuspended in Buffer A2 (10 mM Hepes-KOH pH 7.9, 1.5 mM $MgCl_2$, 10 mM KCL) and incubated on ice for 30 min to allow cell lysis to occur. Nuclei were separated by centrifugation, resuspended in Buffer C2 (20 mM Hepes-KOH pH 7.9, 25 % glycerol, 420 mM NaCl, 1.5 mM $MgCl_2$, 0.2 mM EDTA) and incubated on ice for 30 min, prior to spinning in a table-top centrifuge at 16,100 g, 4 °C for 10 min. The resulting supernatant was dialyzed against Buffer D (20 mM Tris pH 8.0, 20 % glycerol, 0.2 mM EDTA, 100 mM KCl) using a 3,500 molecular weight cutoff dialysis bag overnight. To immunoprecipitate the SWI/SNF complex, 1 ug BRG1 antibody (Santa Cruz #sc-17796) or control IgG antibody were incubated with ~1 mg dialyzed nuclear extract for 2 hrs at 4 °C. The antibody-antigen complex was pulled down in a 2 hr incubation with BSA pre-blotted dynabeads (protein G). To remove any non-specific binders, the dynabeads were washed three times with Tris buffer pH 7.5 containing 300 mM NaCl and 0.5 % NP-40. Before subjecting to iTRAQ MS, the samples were washed one time with 1x PBS and one time with 1/2x PBS. All buffers contained protease inhibitors (Roche) and 1 mM DTT.

iTRAQ mass spectrometry

Tryptic digestion and iTRAQ labeling—The beads for BRG1 and IgG control samples were reconstituted with 20 uL of 50 mM triethylammonium bicarbonate buffer (TEAB). Protease Max Surfactant was added to a final concentration of 0.1 % and *tris*(2-carboxyethyl)phosphine (TCEP) was added to final concentration of 5 mM. Samples were then heated to 55 °C for 20 min, allowed to cool to room temperature and methyl methanethiosulfonate (MMTS) was added to a final concentration of 10 mM. Samples were incubated at room temperature for 20 min to complete blocking of free sulfhydryl groups. 2 ug of sequencing grade trypsin (Promega) was then added to the samples and they were digested overnight at 37 °C. After digestion the supernatant was removed from the beads and was dried in vacuo. Peptides were reconstituted in 50 uL of 0.5 M TEAB, 70 % ethanol and labeled with 8-plex iTRAQ reagent for 2 hrs at room temperature[42]. Labeled samples were then acidified to pH 4 using formic acid, combined and concentrated in vacuo until ~10 uL remained.

2-dimensional fractionation—Peptides were fractionated using a high-low pH reverse phase separation strategy[43]. For the first (high pH) dimension, peptides were fractionated on a 10 cm × 1.0 mm column packed with Gemini 3u C18 resin (Phenomenex, Ventura, CA) at a flow rate of 100 ul/min. Mobile phase A consisted of 20 mM ammonium formate pH 10 and mobile phase B consisted of 90 % acetonitrile, 20 mM ammonium formate pH 10. Samples were reconstituted with 50 uL of mobile phase A and the entire sample injected onto the column. Peptides were separated using a 35 min linear gradient from 5 % B to 70 % B and then increasing mobile phase to 95 % B for 10 min. Fractions were collected every minute for 40 min and were then combined into 8 fractions using the concatenation strategy[44]. Each of the 8 fractions was then separately injected into the mass spectrometer using capillary reverse phase LC at low pH.

Mass spectrometry—An Orbitrap Velos Pro mass spectrometer (Thermo Scientific), equipped with a nano-ion spray source was coupled to an EASY-nLC system (Thermo Scientific). The nano-flow LC system was configured with a 180-μm id fused silica capillary trap column containing 3 cm of Aqua 5-μm C18 material (Phenomenex), and a self-pack PicoFrit™ 100-μm analytical column with an 8-μm emitter (New Objective, Woburn, MA) packed to 15 cm with Aqua 3-μm C18 material (Phenomenex). Mobile phase A consisted of 2 % acetonitrile, 0.1 % formic acid and mobile phase B consisted of 90 % acetonitrile, 0.1 % formic Acid. 3 uL of each sample dissolved in mobile phase A, were injected through the autosampler onto the trap column. Peptides were then separated using the following linear gradient steps at a flow rate of 400 nL/min: 5 % B for 1 min, 5 % B to 35 % B over 70 min, 35 % B to 75 % B over 15 min, held at 75 % B for 8 min, 75 % B to 8 % B over 1 min and the final 5 min held at 8 % B.

Eluted peptides were directly electrosprayed into the Orbitrap Velos Pro mass spectrometer with the application of a distal 2.3 kV spray voltage and a capillary temperature of 275 °C. Each full-scan mass spectrum (Res=60,000; 380–1700 *m/z*) was followed by MS/MS spectra for the top 12 masses. High-energy collisional dissociation (HCD) was used with the normalized collision energy set to 35 for fragmentation, the isolation width set to 1.2 and activation time of 0.1. A duration of 70 sec was set for the dynamic exclusion with an exclusion list size of 500, repeat count of 1 and exclusion mass width of 10 ppm. We used monoisotopic precursor selection for charge states 2+ and greater, and all data were acquired in profile mode.

Database searching—Peaklist files were generated by Mascot Distiller (Matrix Science). Protein identification and quantification was carried using Mascot 2.5[45] against the UniProt human sequence database (89,005 sequences; 35,230,190 residues). Methylthiolation of cysteine and N-terminal and lysine iTRAQ modifications were set as fixed modifications, methionine oxidation and deamidation (NQ) as variable. Trypsin was used as cleavage enzyme with one missed cleavage allowed. Mass tolerance was set at 30 ppm for intact peptide mass and 0.3 Da for fragment ions. Search results were rescored to give a final 1 % FDR using a randomized version of the same Uniprot Human database. Protein-level iTRAQ ratios were calculated as intensity weighted, using only peptides with expectation values <0.05. As this was a protein IP experiment, no global ratio normalization was applied. Protein enrichment was then calculating by dividing the true sample protein ratios by the corresponding control sample ratios.

ChIP-Seq

Library preparation and Illumina sequencing—50 – 100 million cells were crosslinked using 1 % formaldehyde at room temperature for 20 min. Crosslinking was quenched by incubating with 0.125 M glycine for 10 min. ChIP was performed as previously described[46]. Immunoprecipitated DNA was purified using a QIAquick Gel Extraction Kit (Qiagen) and ChIP-Seq libraries were generated using TruSeq ChIP Sample Prep Kit (Illumina) following the manufacturer's instructions. The quality of each library was determined using a Bioanalyzer and High Sensitivity chip (Agilent). Library DNA sizes ranged from 250 to 300 bp. Barcoded libraries were multiplexed at equal molar ratio (two to

six libraries per lane) and sequenced using an Illumina HiSeq 2000 platform as single end reads of 50 bases.

Data analysis—Sequencing reads of 50 bp were mapped to the murine genome assembly mm9 or the human genome assembly hg19 using Bowtie. The MACS peak finding algorithm version 1.4.2 was used to identify ChIP-Seq peaks. H3K27ac and H3K4me3 ChIP-Seq data in RN2 cells was obtained from GSE52277.

Density map generation—In the generation of density plots, all Brg1 peaks with an FDR <0.05 % and a minimal fold enrichment of 5 over input were used. Brg1 peaks were considered as promoters if the peak showed at least 1 bp overlap with a +/− 200 bp window surrounding RefSeq gene transcription start sites (TSSs). If Brg1-enriched peaks showed no overlap with the +/− 200 bp window surrounding RefSeq gene TSSs, they were considered as enhancer-bound peaks. Heatmap matrices were created by counting tags using the indicated window size with 50 bp bins. Heatmap matrices were visualized by Java TreeView 1.1.6r4.

Quantifying FLAG-BRD9 and Brg1 chromatin occupancy after BI-7273 treatment—High confidence peaks (FDR <10 %; minimal fold enrichment of 10 over input) were identified among the DMSO treated FLAG-BRD9 and Brg1 ChIP-Seq data sets. Tag counts for these locations were then re-calculated from uniquely mapped reads in both, DMSO and BI-7273 treated samples, and normalized to the total number of uniquely mapped reads in each data set (to control for differences in sequencing depth). Changes in FLAG-BRD9 and Brg1 chromatin occupancy after BI-7273 exposure were then quantified as the fold change of normalized tag counts between BI-7273 and DMSO treated samples for each of the identified high confidence peaks. To exclude regions of minimal occupancy, peaks with tag counts below 40 and 200 were excluded from the analysis of FLAG-BRD9 and Brg1 binding alterations, respectively.

Plasmids

For competition assays in RN2 cells, LMN-GFP or LMN-mCherry shRNA retroviral vectors were used (MSCV-miR30-shRNA-PGKp-NeoR-IRES-GFP/mCherry). For competition assays in human cell lines, shRNAs were expressed from the MLS-E GFP vector (MSCV-miRE-shRNA-SV40p-GFP)[47]. Conditional RNAi experiments in RN2 cells employed the TRMPV-Neo vector[48]. cDNA constructs were expressed from an MSCV-based vector containing a puromycin resistance gene and a GFP reporter. shRNA sequences used in this study can be found in Supplementary Tables 3 and 4.

Cell culture and virus production

The murine AML line used here (RN2) was derived as previously described[48]. Other cell lines used in this study were obtained from the ATCC or the DSMZ. Murine and human leukemia cells were cultured in RPMI-1640 supplemented with 10 % fetal bovine serum (FBS) and penicillin/streptomycin. iMEF, human solid cancer cell lines, HEK293T and Plat-E cells were cultured in DMEM supplemented with 10 % FBS and penicillin/streptomycin. Cell lines were tested for Mycoplasma contamination once a month.

All retroviral packaging was performed using Plat-E cells according to established protocols. Transient transfection was performed using PEI transfection methods. Virus was collected 48–72 hrs post- transfection.

Competition assay to measure cellular effects of shRNAs

Cells were retrovirally transduced with LMN- or MLS-E shRNA vectors in which shRNA expression is linked to GFP expression through an IRES. The percentage of GFP expressing cells was then measured over various days post-infection using a Guava Easycyte (Millipore). The rate at which the percentage of GFP positive cells declined over time was used to infer the growth disadvantage conferred by a given shRNA relative to the uninfected cells in the same culture.

For cDNA rescue experiments, RN2 cells were first transduced with an MSCV-based vector carrying a transgene and cultured in the presence of puromycin (1 ug/ml) to select infected cells. Cells were subsequently transduced with LMN-shRNA vectors. Double GFP/mCherry positivity was tracked using a BD LSR2 flow cytometer. Data analysis was performed using Flowjo software.

RT-qPCR

Total RNA was extracted from cells using TRIzol (Invitrogen) according to the manufacturer's instructions. Isolating RNA was treated with DNase I to eliminate contaminating genomic DNA. For cDNA synthesis, SuperScript III reverse transcriptase (Life Technologies) was used according to the manufacturer's protocol. All results were quantified by qPCR performed using SYBR green (ABI) on an ABI 7900HT Fast Real-Time PCR machine, and normalized using *Gapdh* as a control gene.

RNA-Seq

Library preparation and Illumina sequencing—Total RNA was extracted using TRIzol reagent (Invitrogen) according to the manufacturer's instructions. RNA-Seq libraries were constructed using the TruSeq sample Prep Kit V2 (Illumina) according to the manufacturer's instructions. Briefly, 2 ug of total RNA were selected with the Poly-A selection procedure and fragmented enzymatically. Poly A-selected and fragmented RNA was further used as template for cDNA systhesis with the Super Script II master mix (Life Technologies). End repairing, dA tailing, adapter ligation and final library amplification steps were subsequently performed. RNA-seq libraries were constructed with "not-so-random" (NSR) primer-based RNA-seq library preparation according to protocols described previously[49]. Briefly, 1 ug of total RNA was used as a template for first-strand synthesis with first-strand primer and Superscript III master mix (Life Technologies), followed by second-strand synthesis with second-strand primer and Klenow fragment. Final amplification of the obtained cDNA was performed with Expand High Fidelity Plus PCR system (Roche). RNA-Seq libraries were sequenced using the Illumina HiSeq 2000 platform. Barcoded libraries were sequenced in a multiplexed fashion of two to six libraries at equal molar ratios, with single end reads of 50 bases.

Data analysis—For the RNAi data set (but not the BRD9 inhibitor data sets), reads were trimmed to 28 bases corresponding to the 9th to 36th position from the 5′ end of the reads for quality purposes. Reads were mapped to mouse genome assembly mm9 or human genome assembly hg19 using Tophat. Differentially expressed genes were identified using Cuffdiff. During this step, structural RNAs (e.g., ribosomal or mitochondrial RNA) were masked. Only genes with FPKM values greater than 5 and 'OK' test status in the control (shRen or DMSO) sample were included in the analysis. For the RNAi data set, the average FPKM value per gene of three independent Brd9 shRNAs was used to calculate the fold change to the shRen control sample. For the BRD9 inhibitor data sets, two independent repeats were performed and fold changes to the shRen control sample were averaged per gene. The graphs show genes plotted from the most down-regulated genes on the left to the most up-regulated genes on the right.

Gene Set Enrichment Analysis (GSEA)—Gene set enrichment analyses were performed using the weighted GSEAPreranked mode according to the instructions at www.broadinstitute.org/gsea/index.jsp. We evaluated all gene sets available through the Molecular Signatures Database containing 15–500 of the differentially expressed genes in our RNA-Seq datasets plus additional custom gene sets, which can be found in Supplementary Data Set 1. A positive Normalized Enrichment Score (NES) reflects enrichment on the left side of the ranked gene list (genes down-regulated with shBrd9 or BRD9 inhibitor), a negative NES reflects enrichment on the right of the ranked gene list (genes up-regulated with shBrd9 or BRD9 inhibitor).

Cell surface marker staining and flow cytometry

RN2 cells transduced with TRMPV-Neo constructs were treated with 0.1 ug/ml doxycycline for 4 days to induce shRNA expression. Cells were then incubated with APC-conjugated Kit (1:200) or Mac-1 (1:200) antibodies in FACS buffer (5 % FBS, 0.05 % NaN_3 in PBS) for 1 hr at 4 °C in the dark. Cells were washed 3x in FACS buffer and then analyzed on a BD LSR2 flow cytometer. Cell surface marker staining was evaluated in GFP^+/$dsRed^+$ (i.e. $shRNA^+$) cell populations. Data analysis was performed using Flowjo software.

May-Grünwald-Giemsa cytospin staining

RN2 cells transduced with TRMPV-Neo constructs were treated with 0.1 ug/ml doxycyclin for 4 days to induce shRNA expression. 50,000 cells were then resuspended in 100 μl FACS buffer (5 % FBS, 0.05 % NaN_3 in PBS) and cytospun onto glass slides using a Shandon Cytospin 2 Centrifuge at 500 rpm for 5 min. May-Grünwald (Sigma) and Giemsa (Sigma) staining was performed according to manufacturer's protocols. Images were collected using a Zeiss Observer Microscope with a 40x objective.

Annexin V staining

Clones derived from RN2 cells transduced with TRMPV-Neo constructs were treated with 0.1 ug/ml doxycycline for 4 days to induce shRNA expression. Annexin V apoptosis staining was then performed according to the manufacturer's protocol (BD, APC Annexin V Apoptosis Detection Kit) and cells were analyzed on a BD LSR2 flow cytometer. Early

apoptotic (Annexin V^+/$DAPI^-$) cells were differentiated from live (Annexin V^-/$DAPI^-$) and dead ($DAPI^+$) cells Data analysis was performed using Flowjo software.

BrdU incorporation assay

Clones derived from RN2 cells transduced with TRMPV-Neo constructs were treated with 0.1 ug/ml doxycycline for 4 days to induce shRNA expression. Cells were then pulsed with BrdU for 30 min and the BrdU incorporation assay was performed according to the manufacturer's protocol (BD, APC BrdU Flow Kit) with DAPI co-staining to measure DNA content. BrdU incorporation and DAPI staining was evaluated in GFP^+/$dsRed^+$ (i.e. $shRNA^+$) cell populations. Data analysis was performed using Flowjo software.

Whole cell lysate preparation and Western blotting

Cell pellets were washed with PBS, resuspended in SDS-PAGE Sample Buffer and passed through a 26.5 gauge needle for 15x prior to boiling at 95 °C for 7 min. The equivalent of 25,000 cells was loaded per lane. Proteins were separated by SDS-PAGE and transferred to a nitrocellulose membrane. The membrane was blocked in 5 % milk for 1 hr at room temperature and then incubated in 1° antibody at 4 °C overnight. The membrane was washed 3x in TBS-T, incubated in 2° antibody for 2 hrs at room temperature, washed another 3x in TBS-T, incubated in ECL and developed.

CRISPR-Screen

CRISPR-Cas9 screening was performed as previously described[50].

Chemical high-throughput screen

The Boehringer Ingelheim proprietary fragment library of ~ 1700 compounds was screened against the BRD9 bromodomain with 3 different assays in parallel: a differential scanning fluorimetry (DSF) assay, a surface plasmon resonance (SPR) assay and a thermophoresis. The hits coming from these three screening methods were validated in an orthogonal binding assay using ^{15}N HSQC NMR (Heteronuclear Single Quantum Coherence Nuclear Magnetic Resonance). 77 hits showed significant cross peak shifts in the ^{15}N HSQC NMR spectra and 55 of these compounds were succsessully co-crystallised with the bromodomain of BRD9. The binding affinity of the compounds was quantified by SPR with 12 compounds displaying a dissociation constant (K_D) of below 100μM. Additionally our proprietary high concentration screening (HiCoS) library of ~ 74,500 compounds was screened virtually with a virtual Glide docking, followed by a BRD9 bromodomain pharmacophore mapping and finally a filtering based on molecular weight (MW<280), lipophilicity (clogP < 2) and compound availability. This virtual screening led to the selection of 208 compounds, which were measured in both our DSF and SPR assays. The binding affinity of the hits was quantified by determination of K_D using SPR. This led to the discovery of 23 additional hits. The binding mode of 11 of these compounds was elucidated by Xray crystallography. In contrast to our fragment library, our HiCoS library is not fully quality controlled for purity, solubility and aggregation; hence all compounds with a K_D below 100μM were resynthesized and all 11 compounds reconfirmed their affinity by SPR remeasurement. Thus 23 fragments with affinity of under 100μM and Xray co-crystal structures were obtained as a

starting point for structure based medicinal chemistry. A more comprehensive description of the derivation of BRD9 inhibitors will be described in a separate study.

Chemical synthesis and characterization

Unless otherwise indicated all reactions were carried out in standard commercially available glassware using standard synthetic chemistry methods. Air-sensitive and moisture-sensitive reactions were performed under an atmosphere of dry nitrogen or argon with dried glassware. Commercial starting materials were used without further purification. Solvents used for reactions were of commercial “dry”- or “extra-dry” or “analytical” grade. All other solvents used were reagent grade.

Preperative RP-HPLC were carried out on Agilent or Gilson systems using columns from Waters (Sunfire C18 OBD, 5 or 10 μm, 20×50 mm, 30×50 mm or 50×150 mm; X-Bridge C18 OBD, 5 or 10 μm, 20×50, 30×50, or 50×150 mm) or YMC (Triart C18, 5 or 10 μm, 20×50 mm, or 30×50 mm). Compounds were eluted with different MeCN/water gradients using either acidic (0.2 % HCOOH or TFA) or basic water (5 mL 2 M NH_4HCO_3 + 2 mL NH_3 (32 %) made up to 1 L with water).

NMR experiments were recorded on Bruker Avance 400 MHz and 500 MHz spectrometers at 298K. Samples were dissolved in 600 μL DMSO-d6 or $CDCl_3$ and TMS was added as an internal standard. 1D 1H spectra were acquired with 30° excitation pulses and an interpulse delay of 4.2 sec with 64,000 datapoints and 20 ppm sweep width. 1D 13C spectra were acquired with broadband composite pulse decoupling (WALTZ16) and an interpulse delay of 3.3 sec with 64,000 datapoints and a sweep width of 240 ppm. Processing and analysis of 1D spectra was performed with Bruker Topspin 2.0 software. No zero filling was performed and spectra were manually integrated after automatic baseline correction. Chemical shifts are reported in ppm on the δ scale.

Analytical LC/MS data [LC/MS(BAS1)] were measured on an Agilent HPLC 1100 Series with Agilent LC/MSD SL detector using a Waters X-Bridge C18, 2.5 μm, 2.1×20 mm column (Part.No. 186003201) and solvent A [20mM NH_4HCO_3/NH_3 (pH 9)] and solvent B [acetonitrile HPLC grade] as eluent (additional settings: flow 1 ml/min; injection volume 5 μl; column temp. 60 °C). Standard gradient: 0.00 min: 10 % B; 0.00 – 1.50 min: 10 % to 95 % B; 1.50 – 2.00 min: 95 % B; 2.00 – 2.10 min: 95 % to 10 % B.

HRMS data were recorded using a Thermo Scientific Orbitrap Elite Hybrid Ion Trap/Orbitrap Spectrometer system with an Ultimate 3000 Series LPG-3400XRS Pump system. The mass calibration was performed using the Pierce LTQ Velos ESI positive ion calibration solution from Thermo Scientific (Lot PF200011, Prod.Nr. 88323).

The synthetic route for BI-7271, BI-7273 and BI-7189 is shown in full in Supplementary Note 2.

AlphaScreen

This assay was used to identify compounds, which inhibit the interaction of the bromodomain of BRD9 with a tetra-acetylated peptide based on the sequence of histone H3

(H3 K9/14/18/23Ac (1–28)). The sequence of the H3 K9/14/18/23Ac(1–28) peptide is Biotin- ARTKQTARK(Ac)STGGK(Ac)APRK(Ac)QLATK(Ac)AARKS, MW: 3392. BRD9 (aa 130 – 259 that contain the bromodomain of BRD9 (accession number NM_023924.4)) was expressed in E. coli with an amino-terminal GST tag. Control BRD4 AlphaScreen assays were performed using a tetra-acetylated H4 tail, which was potently inhibited by JQ1 in control experiments.

The assay was performed in a darkened room below 100 Lux. Compounds are dispensed onto assay plates (Proxiplate-384 PLUS, white, PerkinElmer) using an Access Labcyte Workstation with the Labcyte Echo 550 from a DMSO solution. For the chosen highest assay concentration of 100 μM, 150 nl of compound solution are transferred from a 10 mM DMSO compound stock solution. A series of 11 concentrations is transferred for each compound at which each concentration is five fold lower than the previous one. DMSO is added such that every well has a total of 150 nl compound solution.

10 μl of a mix containing 4 nM GST-BRD9 protein (aa 130 – 259) and 12 nM biotinylated H3 K9/14/18/23Ac(1–28) peptide prepared in assay buffer (50 mM HEPES pH=7.3; 25 mM NaCl; 0,1 % Tween 20; 0.1 % bovine serum albumin (BSA); 2 mM dithiothreitol (DTT)) and 5 μl of bead mix (AlphaLISA Glutathione Acceptor Beads and AlphaScreen Streptavidin Donor Beads mixed in assay buffer at a concentration of 10 μg/ml each) were added to the assay plate that contain 150 nl of the compound solution. After 60 minutes at room temperature the signal was measured in a PerkinElmer Envision HTS Multilabel Reader using the AlphaScreen specifications from PerkinElmer.

Each plate contained negative controls where biotinylated H3 K9/14/18/23Ac(1–28) peptide and GST-BRD9 were left out and replaced by assay buffer. Negative control values were entered as low basis for normalization. IC50 values were calculated using a four parameter non-linear regression model.

BROMOscan

Bromodomain profiling was provided by DiscoveRx Corp. using their BROMOscan platform (http://www.discoverx.com/services/drug-discovery-development-services/epigenetic-profiling/bromoscan). The bromoMAX screen accounted for the determination of the single concentration binding interaction (percent of control - % ctrl) for compound BI-7273 and each of the 32 DNA tagged bromodomains included in the assay by binding competition against a reference immobilized ligand. BromoKdELECT accounted for the determination of the Kd between compound BI-7273 and 11 selected DNA tagged bromodomains by binding competition against a reference immobilized ligand.

NanoBRET

The interactions of the bromodomains of BRD9 with Histone H3.3 were measured by nanoBRET according to the manufacturer's instructions (Promega, products N1830 and N1840). In brief, two chimeric proteins are transiently expressed in HEK293 cells: nanoLuc luciferase fused to the carboxy terminus of the bromodomain of BRD9, and HaloTag fused to the carboxy terminus of histone H3.3. Transfected cells are plated in two sets of triplicates. To the first set of cells, HaloTag 618 ligand is added, a fluorescent small

molecule that selectively binds the HaloTag, The second set of cells does not receive HaloTag 618 ligand. Luciferase substrate is added to all cells. If the bromodomain comes in close proximity of histone H3.3, light emitted at 460 nM by nanoLuc luciferase excites the HaloTag 618 ligand, which then emits at 618 nM. To calculate nanoBRET signals, emission at 618 nM is normalized for emission at 460 nM and divided by the same ratio from cells that did not receive the HaloTag 618 ligand.

Protein purification and crystallization

The bromodomain of human BRD9 (residues 14–134 of isoform 5, Uniprot identifier Q9H8M2-1) was obtained from the SGC (Structural Genomics Consortium) and has been expressed and purified as previously described[51].

Protein crystallization was done using the hanging drop method by mixing 2.0 μL of apo BRD9 (10 mg/mL in 25 mM HEPES pH 7.5, 300 mM NaCl, 0.5 mM TCEP) with 2 μL of reservoir solution (30 % glycerol ethoxylate, 100 mM Tris pH 8.3) at 4 °C. Crystals grew within a few days to a final size of 150–200 μm). Apo crystals were transferred to a soaking buffer containing 33 % glycerol ethoxylate and soaked overnight by adding 0.1 μL of a 100 mM DMSO stock solution of BI-7273. Crystals were frozen in liquid nitrogen and data were collected at the SLS beam line X06SA (Swiss Light Source, Paul Scherrer Institute, λ = 1.000 Å) using the PILATUS 6M detector. The crystals belonged to space group $P2_12_12$ with unit cell parameters a = 70.80, b = 125.34, c = 29.92 and α, β, γ = 90° and contained 2 monomers per asymmetric unit. Images were processed with autoPROC[52]. The resolution limit was set to 1.605 Å using default autoPROC settings. The structure was solved by molecular replacement using the BRD9 structure 3HME as a search model. Subsequent model building and refinement was done with standard protocols using CCP4[53], COOT[54] and autoBUSTER (Global Phasing Ltd.). The structure was refined to R and R_{free} values of 17.8 % and 19.2 %, respectively, with 100 % of the residues in Ramachandran favoured regions as validated with Molprobity[55]. Statistics for data collection and refinement can be found in Supplementary Table 6. PDB: 5EU1.

EC50 measurements

Cells were counted and equal cell numbers were plated and grown in the presence of increasing inhibitor concentrations for 5–7 days. The accumulated cell numbers were then measured using a Guava Easycyte (Millipore) and normalized to cell numbers in DMSO control wells. For profiling of BI-7273 sensitivities across human cancer cell lines in Fig. 4b and Supplementary Fig. 9a, cell viability was assayed using the CellTiter-Glo assay (Promega). EC50 values were calculated using a four parameter non-linear regression model.

ChIP-qPCR

Five million cells were crosslinked using 1 % formaldehyde at room temperature for 20 min. Crosslinking was quenched by incubating with 0.125 M glycine for 10 min. ChIP-qPCR assays were performed as described[46]. Immunoprecipitated DNA was purified using a QIAquick Gel Extraction Kit (Qiagen). All results were quantified by qPCR performed using SYBR green (ABI) on an ABI 7900HT Fast Real-Time PCR machine. Each IP signal

was referenced to an input standard curve dilution series (IP/Input) to normalize for differences in starting cell number and for primer amplification efficiency.

Statistical analysis—P values were determined using the paired, two-tailed Student's T-Test.

Antibodies

Anti-BRG1 (Santa Cruz #sc-17796), Anti-Brg1 (Abcam #ab110641), Anti-Brd9 (Abcam #ab66443), Anti-BRD9 (#ab137245; Bethyl #A303-781A) Anti-β-actin HRP antibody (Sigma #A3854), APC anti-mouse B220 (BioLegend #103212), APC anti-mouse Mac-1/Cd11b (BioLegend #101211), Anti-FLAG (Sigma #F1804), control rabbit IgG (Sigma #I8140)

Databases

All deep-sequencing datasets are available at GEO superseries accession GSE79391. The RNA-seq datasets are available at GEO accession GSE79284. The ChIP-seq datasets are available at GEO accession GSE79360.

The crystal structure of the BRD9 bromodomain bound to BI-7273 is available at PDB: 5EU1.

Supplementary Material

Refer to Web version on PubMed Central for supplementary material.

Acknowledgments

We thank Anand Bhagwat for critical reading of the manuscript and members of the Vakoc lab for discussion of the presented findings. The phylogenetic tree of human bromodomains was kindly provided by Stefan Knapp. This work was supported by Cold Spring Harbor Laboratory NCI Cancer Center Support grant CA455087 for developmental funds and shared resource support. Additional funding was provided by the Alex's Lemonade Stand Foundation, the V Foundation, Pershing Square Sohn Cancer Research Alliance, and by Boehringer-Ingelheim. A.F.H. is supported by a Boehringer Ingelheim Fonds PhD Fellowship. J.S.R. is supported by the Martin Sass Foundation and the Lauri Strauss Leukemia Foundation. C.R.V. is supported by a Burroughs-Wellcome Fund Career Award and National Institutes of Health grant NCI RO1 CA174793.

References

1. Schenone M, Dancik V, Wagner BK, Clemons PA. Target identification and mechanism of action in chemical biology and drug discovery. Nat Chem Biol. 2013; 9:232–40. [PubMed: 23508189]
2. Blagg J, Workman P. Chemical biology approaches to target validation in cancer. Curr Opin Pharmacol. 2014; 17:87–100. [PubMed: 25175311]
3. Arrowsmith CH, et al. The promise and peril of chemical probes. Nat Chem Biol. 2015; 11:536–41. [PubMed: 26196764]
4. Titov DV, Liu JO. Identification and validation of protein targets of bioactive small molecules. Bioorg Med Chem. 2012; 20:1902–9. [PubMed: 22226983]
5. Balzano D, Santaguida S, Musacchio A, Villa F. A general framework for inhibitor resistance in protein kinases. Chem Biol. 2011; 18:966–75. [PubMed: 21867912]
6. Filippakopoulos P, Knapp S. The bromodomain interaction module. FEBS Lett. 2012; 586:2692–704. [PubMed: 22710155]

7. Brand M, et al. Small molecule inhibitors of bromodomain-acetyl-lysine interactions. ACS Chem Biol. 2015; 10:22–39. [PubMed: 25549280]
8. Filippakopoulos P, et al. Histone recognition and large-scale structural analysis of the human bromodomain family. Cell. 2012; 149:214–31. [PubMed: 22464331]
9. Zeng L, et al. Selective small molecules blocking HIV-1 Tat and coactivator PCAF association. J Am Chem Soc. 2005; 127:2376–7. [PubMed: 15724976]
10. Filippakopoulos P, et al. Selective inhibition of BET bromodomains. Nature. 2010; 468:1067–73. [PubMed: 20871596]
11. Nicodeme E, et al. Suppression of inflammation by a synthetic histone mimic. Nature. 2010; 468:1119–23. [PubMed: 21068722]
12. Suzuki A, et al. Aberrant transcriptional regulations in cancers: genome, transcriptome and epigenome analysis of lung adenocarcinoma cell lines. Nucleic Acids Res. 2014; 42:13557–72. [PubMed: 25378332]
13. Hay DA, et al. Discovery and optimization of small-molecule ligands for the CBP/p300 bromodomains. J Am Chem Soc. 2014; 136:9308–19. [PubMed: 24946055]
14. Chen P, et al. Discovery and Characterization of GSK2801, a Selective Chemical Probe for the Bromodomains BAZ2A and BAZ2B. J Med Chem. 2016; 59:1410–24. [PubMed: 25799074]
15. Bennett J, et al. Discovery of a Chemical Tool Inhibitor Targeting the Bromodomains of TRIM24 and BRPF. J Med Chem. 2016; 59:1642–7. [PubMed: 25974391]
16. Shi J, et al. Role of SWI/SNF in acute leukemia maintenance and enhancer-mediated Myc regulation. Genes Dev. 2013; 27:2648–62. [PubMed: 24285714]
17. Buscarlet M, et al. Essential role of BRG, the ATPase subunit of BAF chromatin remodeling complexes, in leukemia maintenance. Blood. 2014; 123:1720–8. [PubMed: 24478402]
18. Hohmann AF, Vakoc CR. A rationale to target the SWI/SNF complex for cancer therapy. Trends Genet. 2014; 30:356–63. [PubMed: 24932742]
19. Oike T, et al. A synthetic lethality-based strategy to treat cancers harboring a genetic deficiency in the chromatin remodeling factor BRG1. Cancer Res. 2013; 73:5508–18. [PubMed: 23872584]
20. Cruickshank VA, et al. SWI/SNF Subunits SMARCA4, SMARCD2 and DPF2 Collaborate in MLL-Rearranged Leukaemia Maintenance. PLoS One. 2015; 10:e0142806. [PubMed: 26571505]
21. Wu JI, Lessard J, Crabtree GR. Understanding the words of chromatin regulation. Cell. 2009; 136:200–6. [PubMed: 19167321]
22. Vangamudi B, et al. The SMARCA2/4 ATPase Domain Surpasses the Bromodomain as a Drug Target in SWI/SNF-Mutant Cancers: Insights from cDNA Rescue and PFI-3 Inhibitor Studies. Cancer Res. 2015; 75:3865–78. [PubMed: 26139243]
23. Kadoch C, et al. Proteomic and bioinformatic analysis of mammalian SWI/SNF complexes identifies extensive roles in human malignancy. Nat Genet. 2013; 45:592–601. [PubMed: 23644491]
24. Middeljans E, et al. SS18 together with animal-specific factors defines human BAF-type SWI/SNF complexes. PLoS One. 2012; 7:e33834. [PubMed: 22442726]
25. Zuber J, et al. Toolkit for evaluating genes required for proliferation and survival using tetracycline-regulated RNAi. Nat Biotechnol. 2011; 29:79–83. [PubMed: 21131983]
26. Subramanian A, et al. Gene set enrichment analysis: a knowledge-based approach for interpreting genome-wide expression profiles. Proc Natl Acad Sci U S A. 2005; 102:15545–50. [PubMed: 16199517]
27. Dhalluin C, et al. Structure and ligand of a histone acetyltransferase bromodomain. Nature. 1999; 399:491–6. [PubMed: 10365964]
28. Zuber J, et al. RNAi screen identifies Brd4 as a therapeutic target in acute myeloid leukaemia. Nature. 2011; 478:524–8. [PubMed: 21814200]
29. Martin LJ, et al. Structure-based design of an in vivo active selective BRD9 inhibitor. J Med Chem. 2016
30. Machleidt T, et al. NanoBRET--A Novel BRET Platform for the Analysis of Protein-Protein Interactions. ACS Chem Biol. 2015; 10:1797–804. [PubMed: 26006698]

31. Clark PG, et al. LP99: Discovery and Synthesis of the First Selective BRD7/9 Bromodomain Inhibitor. Angew Chem Int Ed Engl. 2015; 54:6217–21. [PubMed: 25864491]
32. Theodoulou NH, et al. Discovery of I-BRD9, a Selective Cell Active Chemical Probe for Bromodomain Containing Protein 9 Inhibition. J Med Chem. 2016; 59:1425–39. [PubMed: 25856009]
33. McCabe MT, Creasy CL. EZH2 as a potential target in cancer therapy. Epigenomics. 2014; 6:341–51. [PubMed: 25111487]
34. Margueron R, Reinberg D. The Polycomb complex PRC2 and its mark in life. Nature. 2011; 469:343–9. [PubMed: 21248841]
35. McCabe MT, et al. EZH2 inhibition as a therapeutic strategy for lymphoma with EZH2-activating mutations. Nature. 2012; 492:108–12. [PubMed: 23051747]
36. Neff T, et al. Polycomb repressive complex 2 is required for MLL-AF9 leukemia. Proc Natl Acad Sci U S A. 2012; 109:5028–33. [PubMed: 22396593]
37. Kim W, et al. Targeted disruption of the EZH2-EED complex inhibits EZH2-dependent cancer. Nat Chem Biol. 2013; 9:643–50. [PubMed: 23974116]
38. Winter GE, et al. DRUG DEVELOPMENT. Phthalimide conjugation as a strategy for in vivo target protein degradation. Science. 2015; 348:1376–81. [PubMed: 25999370]
39. Lu J, et al. Hijacking the E3 Ubiquitin Ligase Cereblon to Efficiently Target BRD4. Chem Biol. 2015; 22:755–63. [PubMed: 26051217]
40. Zengerle M, Chan KH, Ciulli A. Selective Small Molecule Induced Degradation of the BET Bromodomain Protein BRD4. ACS Chem Biol. 2015; 10:1770–7. [PubMed: 26035625]
41. Mullard A. Reliability of 'new drug target' claims called into question. Nat Rev Drug Discov. 2011; 10:643–4. [PubMed: 21878966]
42. Ross PL, et al. Multiplexed protein quantitation in Saccharomyces cerevisiae using amine-reactive isobaric tagging reagents. Molecular & cellular proteomics: MCP. 2004; 3:1154–1169. DOI: 10.1074/mcp.M400129-MCP200 [PubMed: 15385600]
43. Gilar M, Olivova P, Daly AE, Gebler JC. Two-dimensional separation of peptides using RP-RP-HPLC system with different pH in first and second separation dimensions. Journal of separation science. 2005; 28:1694–1703. [PubMed: 16224963]
44. Wang Y, et al. Reversed-phase chromatography with multiple fraction concatenation strategy for proteome profiling of human MCF10A cells. Proteomics. 2011; 11:2019–2026. DOI: 10.1002/pmic.201000722 [PubMed: 21500348]
45. Perkins DN, Pappin DJ, Creasy DM, Cottrell JS. Probability-based protein identification by searching sequence databases using mass spectrometry data. Electrophoresis. 1999; 20:3551–3567. DOI: 10.1002/(SICI)1522-2683(19991201)20:18<3551::AID-ELPS3551>3.0.CO;2-2 [PubMed: 10612281]
46. Steger DJ, et al. DOT1L/KMT4 recruitment and H3K79 methylation are ubiquitously coupled with gene transcription in mammalian cells. Molecular and cellular biology. 2008; 28:2825–2839. DOI: 10.1128/MCB.02076-07 [PubMed: 18285465]
47. Fellmann C, et al. An optimized microRNA backbone for effective single-copy RNAi. Cell reports. 2013; 5:1704–1713. DOI: 10.1016/j.celrep.2013.11.020 [PubMed: 24332856]
48. Zuber J, et al. Toolkit for evaluating genes required for proliferation and survival using tetracycline-regulated RNAi. Nature biotechnology. 2011; 29:79–83. DOI: 10.1038/nbt.1720
49. Armour CD, et al. Digital transcriptome profiling using selective hexamer priming for cDNA synthesis. Nature methods. 2009; 6:647–649. DOI: 10.1038/nmeth.1360 [PubMed: 19668204]
50. Shi J, et al. Discovery of cancer drug targets by CRISPR-Cas9 screening of protein domains. Nature biotechnology. 2015; 33:661–667. DOI: 10.1038/nbt.3235
51. Filippakopoulos P, et al. Histone recognition and large-scale structural analysis of the human bromodomain family. Cell. 2012; 149:214–231. DOI: 10.1016/j.cell.2012.02.013 [PubMed: 22464331]
52. Vonrhein C, et al. Data processing and analysis with the autoPROC toolbox. Acta crystallographica. Section D, Biological crystallography. 2011; 67:293–302. DOI: 10.1107/S0907444911007773 [PubMed: 21460447]

53. Collaborative Computational Project, N. The CCP4 suite: programs for protein crystallography. Acta crystallographica. Section D, Biological crystallography. 1994; 50:760–763. DOI: 10.1107/S0907444994003112 [PubMed: 15299374]

54. Emsley P, Lohkamp B, Scott WG, Cowtan K. Features and development of Coot. Acta crystallographica. Section D, Biological crystallography. 2010; 66:486–501. DOI: 10.1107/S0907444910007493 [PubMed: 20383002]

55. Chen VB, et al. MolProbity: all-atom structure validation for macromolecular crystallography. Acta crystallographica. Section D, Biological crystallography. 2010; 66:12–21. DOI: 10.1107/S0907444909042073 [PubMed: 20057044]

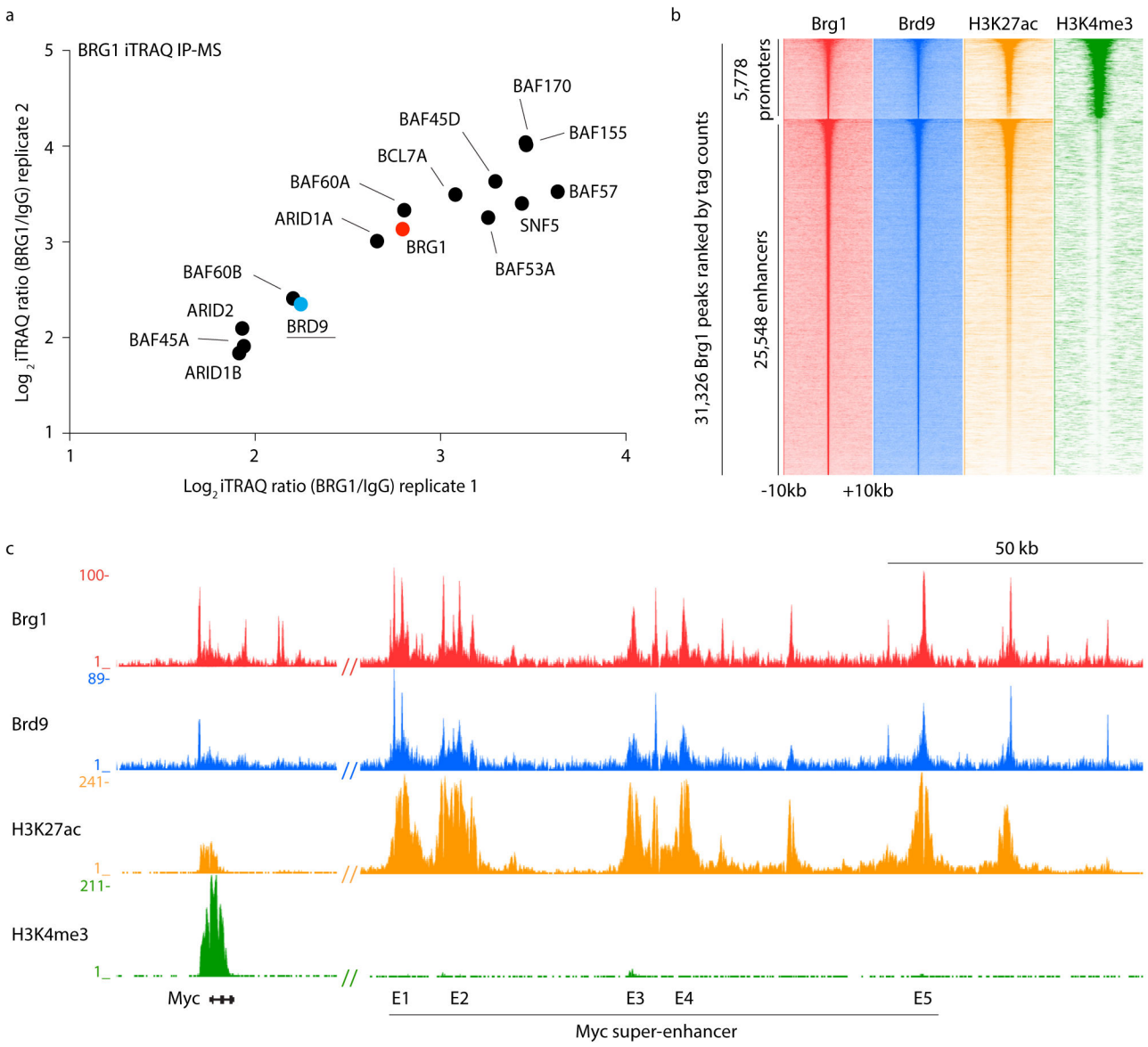

Figure 1. BRD9 is a subunit of SWI/SNF complexes in acute myeloid leukemia cells

(a) iTRAQ IP-MS using BRG1 and IgG antibodies and NOMO-1 cell nuclear extracts to identify BRG1-associated factors. Log-transformed iTRAQ ratios of two independent replicates are plotted for all precipitated proteins previously reported to be part of the SWI/SNF complex[23,24].

(b) Density plot of different ChIP-Seq datasets in RN2 cells centered on Brg1 peaks. Brg1 peaks were identified by MACS peak calling and all peaks with a false discovery rate (FDR) <0.05 % and a fold enrichment over input of greater than 5 were included. The plot depicts tag counts in 50 bp bins in the +/−10 kb region surrounding the Brg1 peak center. Each row represents a single peak.

(c) ChIP-Seq occupancy profiles for Brg1, Brg9, H3K27Ac and H3K4me3 at the *Myc* locus and enhancer in RN2 cells. The y-axis reflects the number of cumulative tag counts within a 50–100 bp bin surrounding each region.

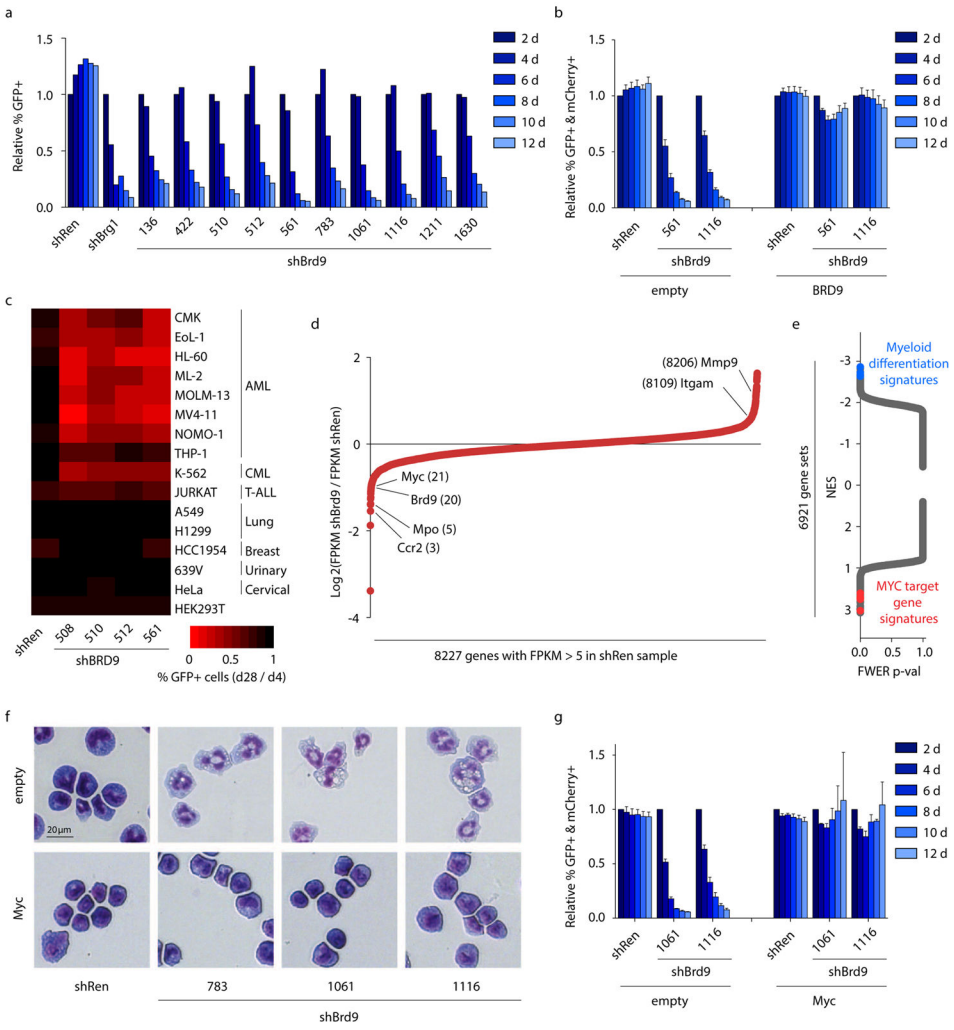

Figure 2. Brd9 supports acute myeloid leukemia growth by sustaining *Myc* expression and an undifferentiated cell state

(a) Competition-based assay to measure effect of shRNAs on growth of RN2 cells. Transduced (shRNA-expressing) cells were identified by co-expression of GFP (LMN vector). The percentage of GFP^+ cells was tracked over 12 days and normalized to GFP percentage on day 2. n = 2

(b) cDNA complementation assay to demonstrate on-target effects of shRNAs. *BRD9* (linked to GFP, MSCV-based vector) was expressed in RN2 cells prior to expression of shRNAs (linked to mCherry, LMN vector). The percentage of double positive cells was tracked and normalized to day 2 values. n = 4

(c) Heatmap summarizing competition-based assay to measure effect of shRNAs on growth of human cancer cell lines. Experiment performed as in (a), except that a MLS-E vector was used and cells were tracked for 28 days. Plotted is the percentage of GFP^+ cells on day 28 normalized to that on day 4. n = 3

(d) RNA-Seq analysis of gene expression changes in RN2 cells expressing Brd9 shRNAs for 2 days (TRMPV-Neo vector). Averaged FPKM values for three independent Brd9 shRNAs were normalized to mRNA levels in control cells expressing shRen.

(e) Gene set enrichment analysis (GSEA) of the RNA-Seq data presented in (d).
(f) Representative light microscopy images of May-Grünwald/Giemsa-stained RN2 cells expressing shRen or shBrd9 for 4 days (TRMPV-Neo vector) in the absence (top) or presence (bottom) of *Myc* expression (MSCV-based vector). Scale bar: 20 μm.
(g) *Myc* cDNA complementation assay. Experiment performed as in (b). n = 3 shRen targets *Renilla* luciferase and serves as a negative control. All error bars in this figure represent SEM.

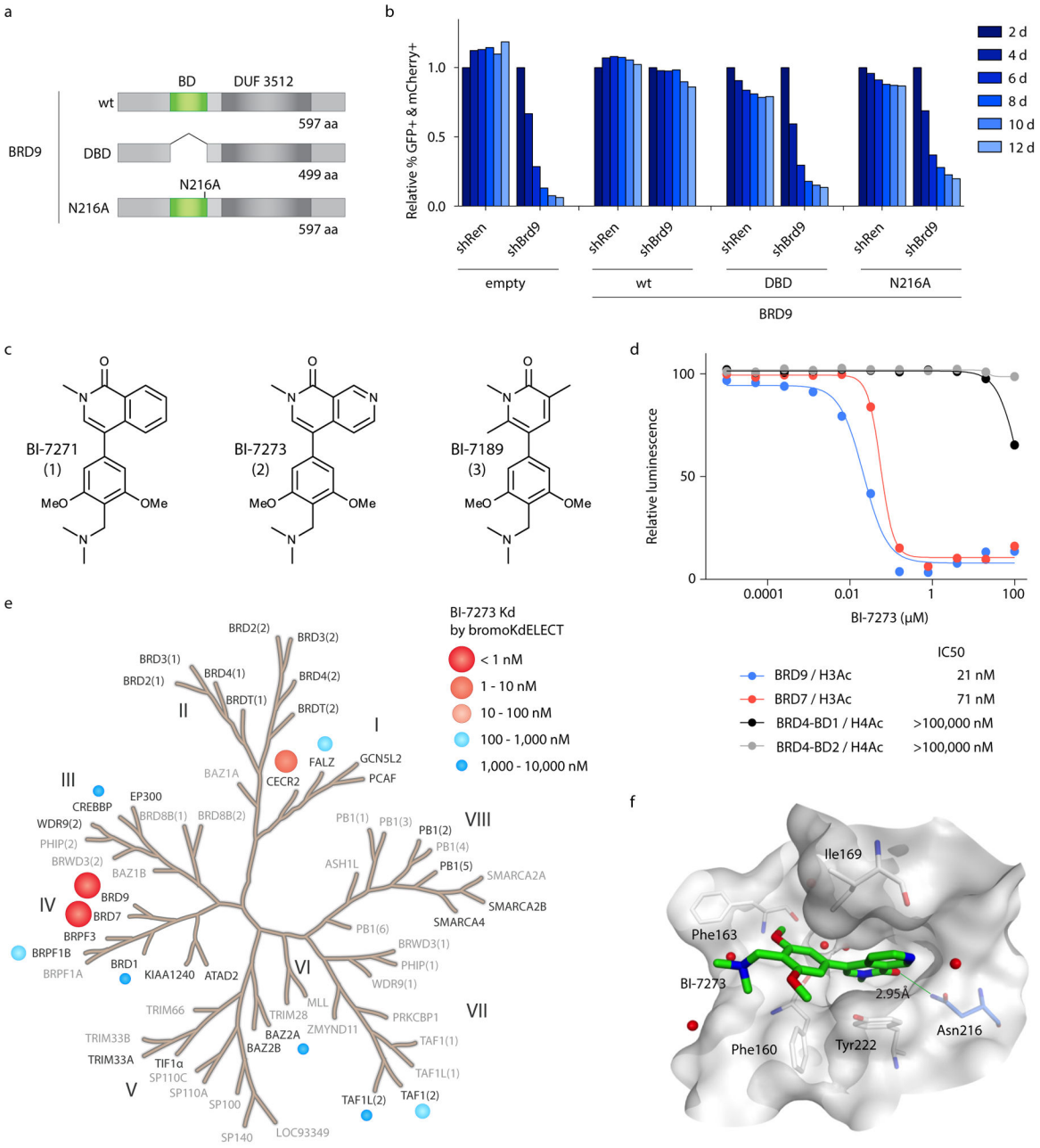

Figure 3. A chemical series that inhibits the BRD9 bromodomain

(a) Domain structure of wild-type (wt) and mutant *BRD9*. BD: Bromodomain, DUF: Domain of Unknown Function, aa: amino acids.

(b) cDNA complementation assay to test functionality of BRD9 mutants. wt or mutant *BRD9* (linked to GFP, MSCV-based vector) was expressed in RN2 cells prior to expression of shRNAs (linked to mCherry, LMN vector). The percentage of double positive cells was tracked and normalized to day 2 values. n = 2

(c) Chemical structures of the BRD9 bromodomain inhibitor series.

(d) AlphaScreen assay to determine binding affinities of BI-7273 for the bromodomains of BRD9, BRD7 and BRD4. Curves were fit by four parameter non-linear regression using the least squares fitting method. Representative graph out of 6–9 replicates is shown.
(e) BROMOscan profiling of BI-7273 binding across the bromodomain family. The bromodomains assayed by bromoMAX are shown in black (pre-configured panel). The depicted affinities were determined by follow-up bromoKdELECT (assaying only those bromodomains identified as binders by bromoMAX).
(f) Co-crystal structure of BI-7273 bound to the BRD9 bromodomain pocket. Key amino acid residues forming the binding pocket are highlighted. The hydrogen bond interaction to Asn216 with 2.95 Å is key for the correct orientation of the ligand. PDB: 5EU1.

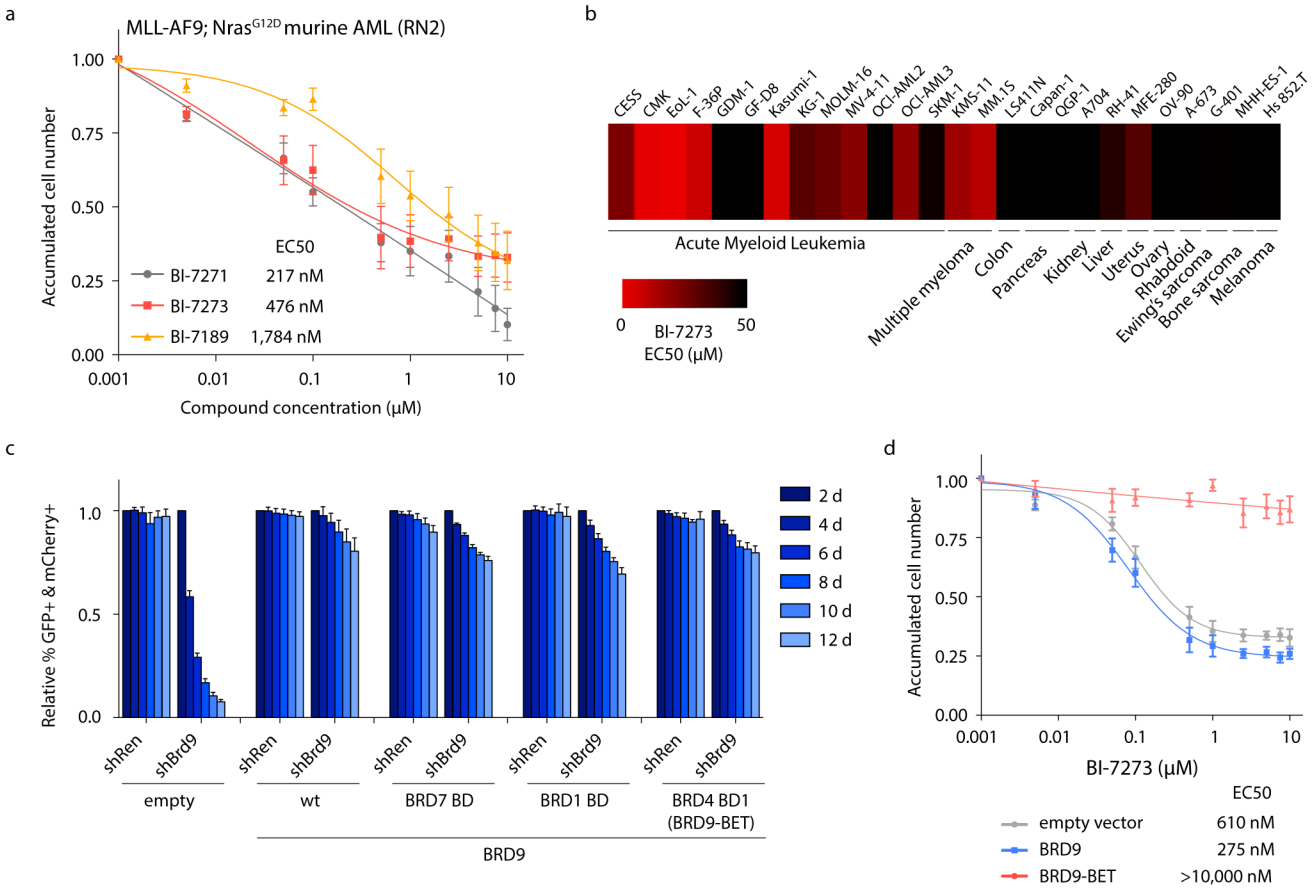

Figure 4. A bromodomain-swap allele validates on-target activity of BRD9 inhibitors

(a) Anti-proliferative effect of BRD9 bromodomain inhibitors on the growth of RN2 cells. RN2 cells were cultured in the presence of increasing inhibitor concentrations for 5 days before cell numbers were determined and normalized to DMSO control. Curves were fit by four parameter non-linear regression using the least squares fitting method. EC50 values were derived from non-linear regression curves with the bottom constrained to 0 and the top constrained to 1. n = 3

(b) EC50 measurements for BI-7273 across human cancer cell lines. Cells were cultured in the presence of increasing BI-7273 concentrations for 7 days before cell proliferation was assessed by CellTiter-Glo and normalized to a DMSO control. n = 2

(c) cDNA complementation assay to test functionality of bromodomain-swap alleles. wt or mutant *BRD9* (linked to GFP, MSCV-based vector) was expressed in RN2 cells prior to expression of shRNAs (linked to mCherry, LMN vector). The percentage of double positive cells was tracked and normalized to day 2 values. shRen targets *Renilla* luciferase and serves as a negative control. n = 5

(d) Cell counts to measure the effect of BI-7273 on the growth of RN2 cells transduced with and selected for empty vector, *BRD9* or BRD9-BET (MSCV-based vector). Experiment performed as in (a). n = 3

All error bars in this figure represent SEM.

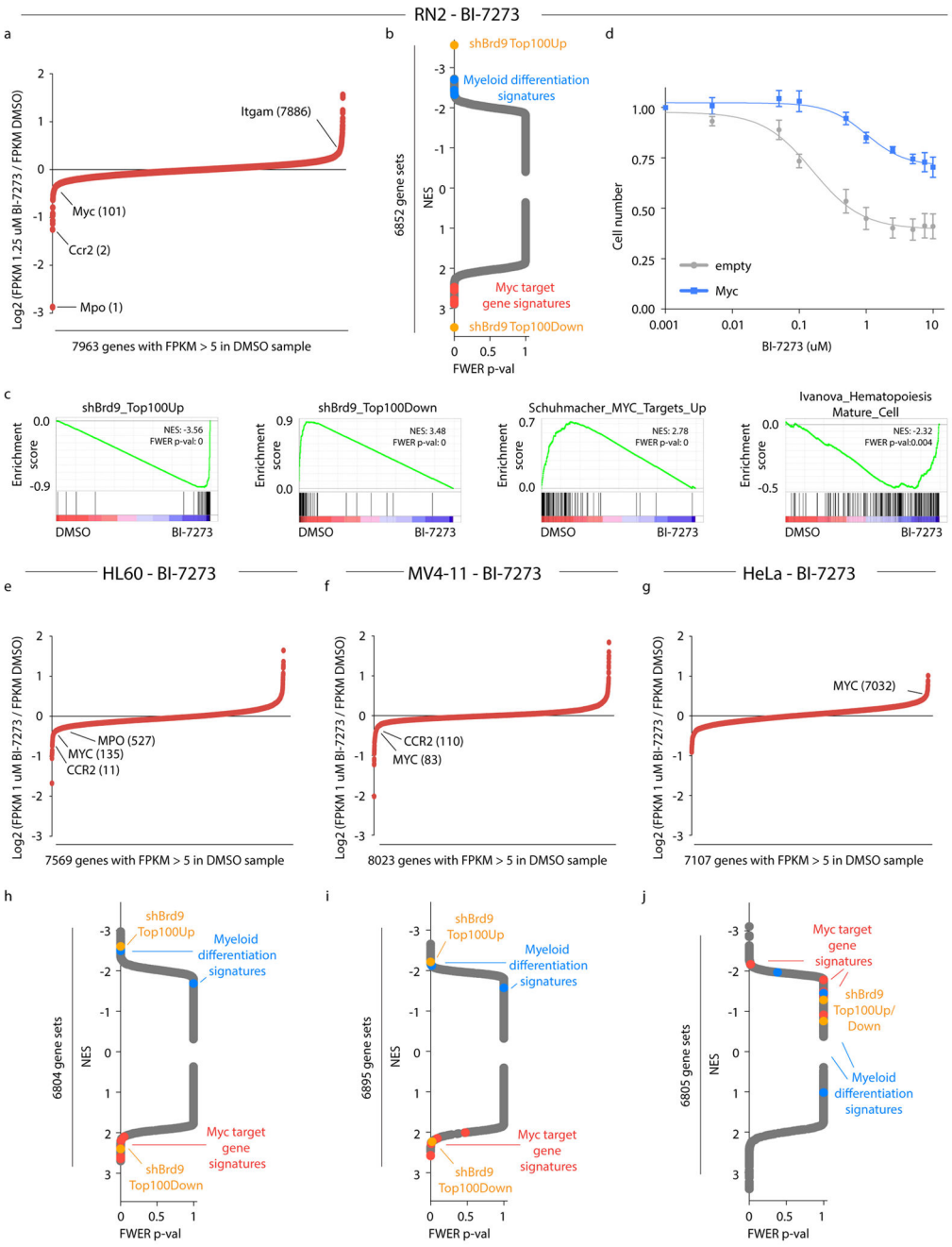

Figure 5. Chemical Brd9 inhibition mimics the transcriptional effects of Brd9 knockdown

(a) RNA-Seq analysis of gene expression changes in RN2 cells after 24 hours of 1.25 μM BI-7273 exposure. FPKM values from treated cells were normalized to FPKM values recorded in cells cultured in presence of DMSO. n = 2

(b) Gene set enrichment analysis (GSEA) of RNA-Seq data presented in (a).

(c) GSEA plots of the top 100 genes up- and down-regulated after 2 days of shBrd9 expression in RN2 cells (shBrd9_Top100Up, shBrd9_Top100Down), genes up-regulated in Burkitt's Lymphoma cells induced to express MYC (Schuhmacher_MYC_Targets_Up) and

genes up-regulated in mature blood cell populations from adult bone marrow and fetal liver (Ivanova_Hematopoiesis_Mature_Cell).

(d) Cell counts to measure effect of BRD9 bromodomain inhibitors on growth of RN2 cells transduced with and selected for empty vector or *Myc* (MSCV-based vector). Cells were cultured in the presence of increasing inhibitor concentrations for 5 days before cell numbers were determined and normalized to DMSO control. Curves were fit by four parameter nonlinear regression using the least squares fitting method. n = 3

(e, f, g) RNA-Seq analysis of gene expression changes in HL60 (e), MV4-11 (f) and HeLa (g) cells after 24 hours of 1 μM BI-7273 exposure. FPKM values from treated cells were normalized to FPKM values recorded in cells cultured in the presence of DMSO. n = 2

(h, i, j) Gene set enrichment analysis (GSEA) on the RNA-Seq data presented in (e), (f) and (g), respectively.

FWER p-val, familywise-error rate p-value.

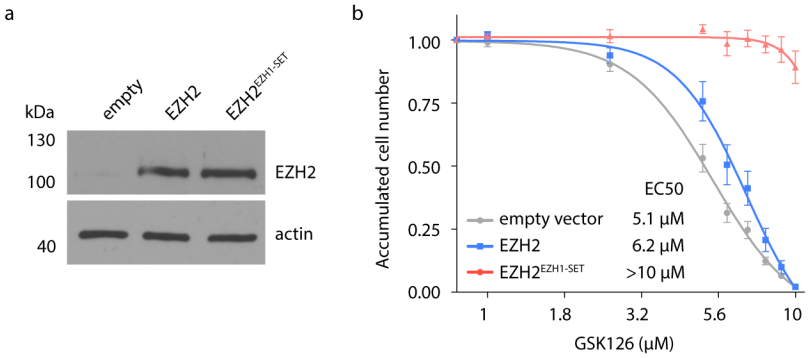

Figure 6. A SET domain-swap allele validates on-target activity of the EZH2 inhibitor GSK126

(a) Western blot to test expression of *EZH2* wt and *EZH2*$^{EZH1\text{-}SET}$ in RN2 cells. The antibody recognizes human EZH2 exclusively. For this reason no Ezh2 band is observed in the 'empty' lane. The actin blot serves to control for loading. Uncropped images can be found in Supplementary Fig. 15b.

(b) Cell counts to measure the effect of EZH2 inhibitor GSK126 on the growth of RN2 cells transduced with and selected for empty vector, *EZH2* or *EZH2*$^{EZH1\text{-}SET}$ (MSCV-based vector). Cells were cultured in the presence of increasing inhibitor concentrations for 7 days before cell numbers were determined and normalized to DMSO control. Curves were fit by four parameter non-linear regression using the least squares fitting method. EC50 values were derived from non-linear regression curves with the bottom constrained to 0 and the top constrained to 1. n = 5